Eur. Phys. J. A **24**, 185–191 (2005)
DOI 10.1140/epja/i2005-10007-5

THE EUROPEAN PHYSICAL JOURNAL A

Theoretical simulation for identical bands

Y.J. Chen[1,a], Y.S. Chen[2], C.W. Shen[2], Z.C. Gao[2], S.J. Zhu[1], and Y. Tu[2]

[1] Department of Physics, Tsinghua University, Beijing 100084, PRC
[2] China Institute of Atomic Energy, Beijing, 102413, PRC

Received: 27 January 2005 /
Published online: 11 April 2005 –
Communicated by G. Orlandini

Abstract. The frequency of occurrence of identical bands in superdeformed and normal-deformed nuclei is studied by carrying out a statistical analysis of a large number of rotational bands, which are generated with the reflection asymmetric shell model. The frequency of occurrence and the behaviors of identical bands revealed in the statistical analysis of the experimental bands were generally reproduced by the present theoretical simulation. This would indicate that the nuclear mean-field approximation plus the beyond mean-field one, like angular-momentum and parity projections, can explain the phenomena of identical bands even though there is no available theory that can reach the accuracy of identity between the specific identical bands. Furthermore, the octupole effect on the identical bands is discussed. The present theoretical simulation shows that more correlations may lead to more identical bands.

PACS. 21.60.Cs Shell model – 21.10.-k Properties of nuclei; nuclear energy levels – 27.70.+q $150 \leq A \leq 189$ – 27.80.+w $190 \leq A \leq 219$

1 Introduction

The fascinating phenomenon of identical bands (IBs) was first discovered in 1990 [1]. This came as a complete surprise and initialized many new experimental studies. Shortly afterwards, several other superdeformed (SD) IBs in the Hg region [2,3] were found, and then this phenomenon has also been seen in normal-deformed (ND) nuclei [4]. Since then, a number of IBs were observed at both low and high spins, and they span different shapes in several mass regions. Following these experimental findings, many efforts have been made to understand the nature and origin of this phenomenon [5]. In ref. [6] the frequency of occurrence of the IBs in the experiment was investigated, and it was pointed out that IBs are much more frequently occurring in SD than in ND nuclei and the main reason for this striking difference was attributed to the significant differences in the pairing properties between SD and ND nuclei. In ref. [7] the occurrence of IBs was studied based on the Cranked Nilsson-Strutinsky model, despite the conclusion is in line with that of the experimental statistics [6], the disadvantage of this model is clear, namely the angular momentum is not a good quantum number, and the calculations of this model cannot be directly compared with the measured energy levels of rotational bands.

Recently, the reflection asymmetric shell model (RASM) has been formulated [8]. This makes it possible to simulate theoretically the frequency occurrence of IBs in heavy and SD nuclei at the microscopic level of the shell model. Within the RASM, the calculated rotational bands have good angular momentum and good parity just like experimental rotational bands except the fact that parity and spins have not been assigned for the majority of experimental SD bands. The RASM follows the basic idea of the standard shell model and the octupole coupling force is included in the Hamiltonian. In SD nuclei, the octupole correlations were found in experiment as a universal phenomenon in the $A = 190$ and 150 regions, see, for example, ref. [9] and ref. [10]. Therefore, for a more realistic theoretical simulation for SD rotational bands in the $A = 190$ region, the octupole correlation should be considered. The RASM is the only shell model that can be used to describe the octupole SD nuclei. Thus, in our theoretical simulation of IBs in SD nuclei and ND nuclei, the RASM is employed to generate rotational bands.

To identify a pair of IBs, we have to choose a criterion to define the IBs. The term "identical band" has been used in several different ways. Someone applied it to a pair of bands having the same dynamic moments of inertia $J^{(2)}$, while others have restricted its use to a pair of bands having the same actual γ-ray energies E_γ. Recently, a convenient way, so-called energy factor method, has been proposed to generalize the definition of IBs, which, to a large degree, combines the two most common criterions,

[a] e-mail: yj-chen@mail.tsinghua.edu.cn

namely the requirements of near equality of the gamma-ray energies and the dynamic moments of inertia of two bands, into one [11,12]. This method is employed to define the IBs in the present study. We will see later that the results and conclusions would not be changed if alternative reasonable criterions were chosen.

The purpose of the present work is to make a theoretical simulation to study the statistical properties of IBs. First, the rotational bands are generated by RASM calculations for a considerable large number of SD and ND nuclei. Second, statistical studies for IBs are carried out by means of the energy factor method. In the present work, we shall show that the large deformation effect on the occurrence of IBs is already embedded in the nuclear deformed mean field, like the one described by the Nilsson potential. One of the goals of the present study is to show that the frequency of occurrence and the properties of IBs, such as the quantization of incremental alignments revealed in the statistical analysis of the experimental rotational bands, can be generally reproduced within the mean-field approximation including BCS pairing, although not any available theoretical model based on and beyond the mean-field approximation can describe the matter with the accuracy of the identity between the observed specific IBs, *i.e.* $\Delta E_\gamma \approx 1$ keV.

The paper is organized as follows. In sect. 2 and sect. 3, the reflection asymmetric shell model and the energy factor method are briefly introduced. The results of simulation and the incremental alignments of IBs are discussed in sect. 4. A summary is given in sect. 5.

2 Brief description of the reflection asymmetric shell model

In the reflection asymmetric shell model the simultaneous angular-momentum and parity projections are carried out with a chosen set of Nilsson + BCS states and then the projected states are used to diagonalize the spherical shell model Hamiltonian. With such projected basis the truncation of the many-body basis can be achieved so that the shell model calculation can be performed for heavy and superdeformed nuclei. The validity of the RASM has been demonstrated by a good description of the properties of the octupole bands in Ra isotopes [8]. For an axial but non-octupole shape, rotational bands can also be calculated with the RASM by setting the octupole deformation parameter ε_3 to be zero, namely the model is reduced to the projected shell model (PSM) [13].

In the RASM, we consider a set of deformed BCS multi-quasiparticle states $\{|\Phi_\kappa\rangle\}$, where κ denotes the quasiparticle configurations. Then the trial wave function $|\Psi\rangle$ can be constructed as the superposition of oriented in space and the "left-right" to "right-left" reflected intrinsic wave functions,

$$|\Psi\rangle = \sum_{IMK\kappa p} F^{Ip}_{MK} P^p P^I_{MK\kappa} |\Phi_\kappa\rangle , \tag{1}$$

where $\hat{P}_{MK\kappa}(P^p)$ is the angular-momentum (parity) projection operator. The $\{P^p P^I_{MK} |\Phi_\kappa\rangle\}$ is the set of simultaneously angular-momentum– and parity–projected multi-quasiparticle states, which forms the shell model space, and the coefficients F^{Ip}_{MK} are determined by diagonalizing the shell model Hamiltonian, namely solving the following eigenvalue equation:

$$\sum_{K\kappa} \{\langle\Phi_{\kappa'}| H P^p P_{K'K} |\Phi_\kappa\rangle - E^{Ip} \langle\Phi_{\kappa'}| P^p P_{K'K} |\Phi_\kappa\rangle\} F^{Ip}_{MK\kappa} = 0, \tag{2}$$

with the normalization condition

$$\sum_{K'\kappa' K\kappa} F^{Ip*}_{MK\kappa} \langle\Phi_{\kappa'}| P^p P_{K'K} |\Phi_\kappa\rangle F^{Ip}_{MK\kappa} = 1. \tag{3}$$

The Hamiltonian is written as

$$\hat{H} = \hat{H}_0 - \frac{1}{2}\sum_{\lambda=2}^{4} \chi_\lambda \sum_{\mu=-\lambda}^{\lambda} \hat{Q}^+_{\lambda\mu}\hat{Q}_{\lambda\mu} - G_M \hat{P}^+_{00}\hat{P}_{00} - G_Q \sum_{\mu=-2}^{2} \hat{P}^+_{2\mu}\hat{P}_{2\mu} , \tag{4}$$

where $\hat{H}_0$ is the spherical single-particle shell model Hamiltonian, the second term includes the quadrupole ($\lambda = 2$), octupole ($\lambda = 3$) and hexadecapole ($\lambda = 4$) interactions, which lead to the quadrupole, octupole and hexadecapole deformations, respectively, the third and fourth terms represent the monopole and quadrupole pairing interactions, respectively. The coupling constants, χ_λ, can be determined consistently with the deformations [8]. The monopole pairing strength constant G_M may be calculated by

$$G_M = \left[g_1 \mp g_2 \left(\frac{N-Z}{A}\right)\right] \times A^{-1}, \tag{5}$$

where the minus (plus) sign represents the neutron (proton). In the present calculations $g_1 = 21.24$ and $g_2 = 13.86$ were taken for the SD nuclei in the $A = 190$ mass region and the ND nuclei in rare-earth region. The quadrupole pairing strength G_Q is assumed to be proportional to the monopole strength, $G_Q = f_Q G_M$. In the present work we set $f_Q = 0.2$ for SD nuclei and 0.16 for ND nuclei. The Nilsson parameters κ and μ are taken from ref. [14]. The calculations include three major shells $N = 5, 6$ and 7 (4, 5 and 6) for neutrons (protons) for SD nuclei and $N = 4, 5$ and 6 (3, 4 and 5) for neutrons (protons) for ND nuclei. The deformation parameters were taken as $\varepsilon_2 = 0.41$–0.45, $\varepsilon_3 = 0.062$ for SD nuclei in the $A = 190$ region, $\varepsilon_2 = 0.2$ for ND nuclei in the rare-earth region. These quadrupole deformation parameters have been adopted by systematically considering the previous works, and also by fitting approximately the yrast bands of the considered specific nuclei. The octupole deformation $\varepsilon_3 = 0.062$ has been used in RASM calculation to reproduce the parity splitting between the observed parity partner, for example, the negative-parity SD band 3 and the yrast SD band 1 in ^{194}Hg [9].

3 The energy factor method for identical bands

With the calculated rotational bands, we employ the so-called energy factor method [11] to study the frequency occurrence of IBs, and the method is briefly introduced in the following. We select the regions of bands A and B, each band consists of $N+1$ consecutive transition energies $E_\gamma(I_A)$ and $E_\gamma(I_B)$, and then compare the two quantities $E'_\gamma(I_A)$ and $E_\gamma(I_B)$. Here $E'_\gamma(I_A)$ is defined, by introducing the energy factor χ, as

$$E'_\gamma(I_A) = \chi E_\gamma(I_A) + (1-\chi)E_\gamma(I_A+2), \tag{6}$$

$$(I_A = I_A^0 + 2k, I_B = I_B^0 + 2k, k = 0, 1, 2, 3, ..., N-1). \tag{7}$$

where the χ is restricted to [0,1], I_A^0 and I_B^0 are the band head spin for the bands A and B, respectively. The transition energy at the band head in the band B satisfies the relation $E_\gamma(I_A^0) \leq E_\gamma(I_B^0) \leq E_\gamma(I_A^0+2)$. In fact, the factor χ describes the relationship of the transition energies of the bands A and B, and it can be determined by minimizing the quantity s,

$$s = \sum_{k=0}^{N-1} [E'_\gamma(I_A) - E_\gamma(I_B)]^2, \tag{8}$$

and the result is

$$\chi = \frac{\sum\limits_k [E_\gamma(I_A+2) - E_\gamma(I_A)][E_\gamma(I_A+2) - E_\gamma(I_B)]}{\sum\limits_k [E_\gamma(I_A+2) - E_\gamma(I_A)]^2}. \tag{9}$$

For an appropriate N and δ, if $\left|E'_\gamma(I_A) - E_\gamma(I_B)\right| \leq \delta$ is fulfilled for all k's, the two bands are then regarded as IBs.

The energy factor method is a useful tool in making a systematic study of IBs. One of the advantages of this method is that the average value of the incremental alignment of IBs can be directly calculated from the energy factor. For a pair of IBs, the incremental alignment Δi is defined in ref. [15] as

$$\Delta i = 2\frac{E_{\gamma\,\mathrm{near}} - E_\gamma(I_B)}{E_\gamma(I_A+2) - E_\gamma(I_A)}, \tag{10}$$

where $E_{\gamma\,\mathrm{near}}$ is the transition energy in the band A which is the closest to the $E_\gamma(I_B)$ in the band B, and band A is supposed to be a reference band. From eqs. (6), (8), (9) and the assumption that δ is almost a constant value for the rotational band, we could find the relation between χ and $\overline{\Delta i}$ (the arithmetic average of Δi which is equivalent to $\frac{1}{N}\sum \Delta i(k)$:

$$\overline{\Delta i} \approx 2\chi \tag{11}$$

if $E_{\gamma\,\mathrm{near}} = E_\gamma(I_A+2)$ and

$$\overline{\Delta i} \approx 2(\chi - 1) \tag{12}$$

if $E_{\gamma\,\mathrm{near}} = E_\gamma(I_A)$. The rule for choosing eq. (10) or eq. (11) to calculate $\overline{\Delta i}$ is that eq. (10) is used if $2\chi \in [-1, +1]$, otherwise, eq. (11) is used. Here, the incremental alignments Δi and its average values $\overline{\Delta i}$ are restricted to the region $[-1, +1]$.

The quantized incremental alignment between pairs of IBs in nuclei of the same type (both even mass or both odd mass) is integer (including zero), and is half-integer between bands in nuclei of different types [16]. In the present work, all considered nuclei are even-even nuclei, and thus the incremental alignment of IBs which varies around $-1.0, 0, 1.0$ shows the feature of quantization [3]. But there is no demarcation line between the quantization and non-quantization of the incremental alignment. Because the incremental alignments vary against the transition energies E_γ and the average incremental alignment ($\overline{\Delta i}$) for a pair of IBs cannot be precisely $-1.0, 0, 1.0$, we divide the region $[-1, +1]$ into two kinds of regions as the following: the quantized region Q,

$$Q = \left[-1, -\frac{3}{4}\right] \cup \left(-\frac{1}{4}, +\frac{1}{4}\right] \cup \left(\frac{3}{4}, 1\right] \tag{13}$$

which consists of three subregions centered at $-1.0, 0, 1.0$ and the unquantized region U which is around ± 0.5. This means that the Q region and the U region are treated equally. The incremental alignment of IBs is regarded as quantized if its $\overline{\Delta i}$ lies within the Q region, otherwise it is unquantized.

4 Results and discussions

4.1 The occurrence of IBs in SD and ND nuclei

We are primarily interested in the frequency of occurrence of IBs in SD nuclei. The IBs in ND nuclei are not well defined in contrast to those in SD nuclei, but it is better to make comparisons between SD and ND nuclei in order to gain the insight into the phenomena. In the present study, 13 ND nuclei in the $A = 160$ region (rare-earth region), 8 SD nuclei in the $A = 190$ region are included, and they all are even-even nuclei. For SD nuclei where the octupole correlation is taken into account, the calculation of RASM will generate two kinds of rotational bands, *i.e.*, the bands with positive parity and the bands with negative parity. The considered SD nuclei are ^{190,192,194}Hg, ^{192,194,196,198}Pb, and ^{198}Po in the $A = 190$ region, and the considered normal-deformed nuclei are ^{166,168,170,172,174,176}Yb, and ^{166,168,170,172,174,176,178}Hf in the rare-earth region. In this work, 10 positive-parity and 10 negative-parity low-lying bands are calculated for each considered SD nucleus, and 20 low-lying bands are calculated for each considered ND nucleus, thus we shall have 160 SD bands and 260 ND bands for the analysis, and these calculated rotational bands have good angular momentum and good parity just like experimental rotational bands except for the fact that parity and spins have not been assigned for the majority of experimental SD bands. Consequently, the possible effects on the frequency of occurrence of IBs from deformations, rotations, intruder high-j orbits and pairing correlations can be studied.

Table 1. The numbers of the calculated ND IBs vary against N and δ in the $A = 160$ (rare-earth) region.

A	δ	N							
	(keV)	6	7	8	9	10	11	12	13
	0.5	43	13	6	3	1	0	0	0
	1.0	212	78	30	11	7	3	1	1
160	1.5	423	204	85	39	15	8	4	1
	2.0	676	346	170	85	40	20	9	7
	2.5	1006	533	275	148	79	34	16	8
	3.0	1411	740	414	219	129	59	29	14

Table 2. The numbers of the calculated SD IBs vary against N and δ in the $A = 190$ mass region corresponding to $\varepsilon_3 = 0.062$.

A	δ	N							
	(keV)	8	9	10	11	12	13	14	15
	0.5	465	252	146	83	50	30	17	6
	1.0	1650	1023	614	386	231	141	81	46
190	1.5	2580	1916	1308	828	555	345	223	137
	2.0	3697	2814	2021	1369	936	639	415	276
	2.5	4401	3487	2692	1965	1390	970	656	441
	3.0	4982	4113	3270	2499	1864	1259	945	641

The results of the statistical analysis for IBs with the calculated bands are given in table 1 and table 2, where the number of IBs *versus* N and δ are shown. It is seen that the number of IBs decreases with increasing N and/or with decreasing δ for both the ND and SD nuclei. There is a large difference between the numbers of IBs in the SD and ND nuclei for given N and δ. For example, the number of IBs is 85 for the ND bands and 2580 for the SD bands in the $A = 190$ region at $N = 8$ and $\delta = 1.5$ keV. These statistical properties of IBs presented in the present theoretical simulations are just what we have seen in the experiment, at least qualitatively.

From tables 1 and 2, we can see that the frequency of occurrence of IBs in SD nuclei is much higher than that in ND nuclei. This may be explained by means of the interplay between the deformation, pairing, rotation and the alignments of quasiparticles, which present large differences in SD and ND nuclei. ND nuclei have a smaller deformation and relative low rotational frequency, the pairing is much stronger than that for SD nuclei, therefore the alignments of quasiparticles occur quickly and contribute significantly to the $J^{(2)}$ moment of inertia. Consequently, the distribution of the moments of inertia should be broader in ND nuclei than in SD nuclei (as shown in fig. 1). In contrast, SD nuclei possess a large deformation, the pairing correlation is expected to be very weak and the high-N intruder orbits have the most important influence on the $J^{(2)}$ moments of inertia, and other orbits are very less perturbed by the rotation and thus contribute less to the $J^{(2)}$. Consequently, the distribution of the $J^{(2)}$ moments of inertia should be narrower in SD nuclei than in ND nuclei. Therefore, the occurrence of IBs in SD nuclei is more frequent than that for ND nuclei. We shall see, indeed, that the calculated distributions of the $J^{(2)}$, as well as the E_γ, show such a difference between SD and ND nuclei.

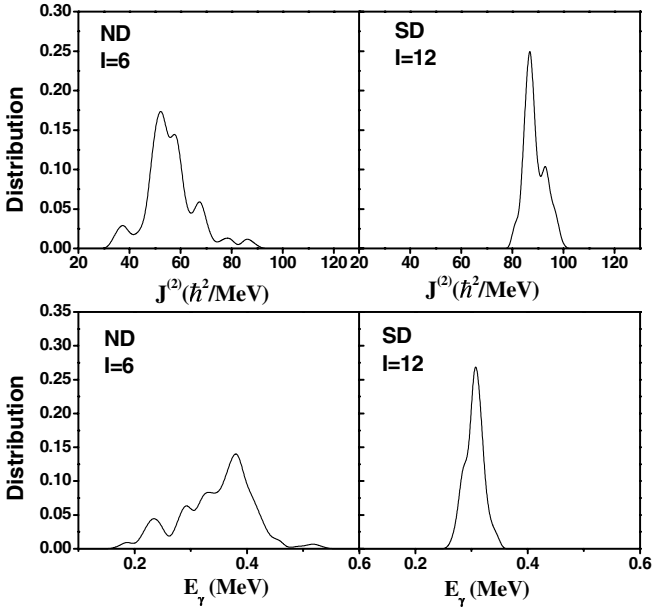

Fig. 1. Distribution functions of the calculated $J^{(2)}$ (upper part) and γ-ray energies E_γ (lower part), at spin 6 for ND bands in the rare-earth region and spin 12 for SD bands in the $A = 190$ mass region.

Once the rotational bands are calculated with the RASM, namely $E(I^\pi)$, the γ transition energies of each band are then obtained to be $E_\gamma(I^\pi) = E(I^\pi + 2) - E(I^\pi)$ and the dynamic moment of inertia can be calculated to be $J^{(2)}(I^\pi) = (\mathrm{d}^2E(I^\pi)/\mathrm{d}I^2)^{-1} \approx 4/\Delta E_\gamma(I^\pi)$, where $\Delta E_\gamma(I^\pi) = E_\gamma(I^\pi) - E_\gamma(I^\pi - 2)$. The only difference between theoretical and experimental situations is that spins

Table 3. The numbers of the calculated SD IBs against N and δ in the $A = 190$ region corresponding to $\varepsilon_3 = 0$.

A	δ	N							
	(keV)	8	9	10	11	12	13	14	15
	0.5	324	185	120	71	40	30	19	15
	1.0	1020	638	398	260	169	109	83	56
190	1.5	1785	1220	804	533	349	260	172	119
	2.0	2467	1789	1273	879	582	407	290	202
	2.5	3107	2288	1695	1237	891	600	417	306
	3.0	3456	2740	2104	1599	1182	849	580	412

are not assigned for most of the experimental SD bands, while the SD states generated by the RASM have good angular momentum and parity. Therefore, the calculated quantities in the present work are functions of spin, and we do not need to introduce a classical term, *i.e.*, the rotational frequency which has been widely used in the analysis of experimental SD bands. Figure 1 shows the distributions of calculated $J^{(2)}$ moments of inertia (upper part) and γ-ray energies E_γ (lower part) at spin 6 for ND nuclei in the rare-earth region and at spin 12 for SD nuclei in the $A = 190$ region. The selections of spin 6 in the ND case and spin 12 in the SD case are not specific requirements, but warrant no occurrence of backbending and thus a meaningful comparability. It is seen from fig. 1 that the distribution for $J^{(2)}$ as well as for E_γ is much broader for ND nuclei than that for SD nuclei. This implies that the probability to find similar values either of E_γ or of $J^{(2)}$, namely to obtain the IBs in superdeformed nuclei, is larger than that in normal-deformed nuclei.

To investigate the effect of the octupole deformation on the frequency of occurrence of IBs, we have also performed a similar statistical analysis for SD IBs in the $A = 190$ region by setting the octupole deformation parameter ε_3 to be zero in the RASM calculations, *i.e.*, the SD nuclei are axial but of non-octupole shape in the following calculations. We still select 20 low-lying bands for each considered nucleus, and the considered nuclei still are ^{190,192,194}Hg, ^{192,194,196,198}Pb, and ^{198}Po. The results of the numbers of IBs are shown in table 3.

By comparing tables 2 and 3, we can see that the conclusion that the number of IBs decreases with increasing N and/or decreasing δ would not change if the octupole correlation is switched off. However, the numbers of identical bands *versus* N and δ are different for the cases of $\varepsilon_3 = 0$ and $\varepsilon_3 = 0.062$. For example, the number of IBs is 349 for $\varepsilon_3 = 0$ and 555 for $\varepsilon_3 = 0.062$ in the $A = 190$ region at $N = 12$ and $\delta = 1.5$ keV. This indicates that under the same criterion conditions, the numbers of IBs increase in the presence of octupole deformation. This may be attributed to the octupole-deformation–induced fragmentation effect on the quasiparticle alignments [17]. The octupole correlation between the high-j unique-parity and normal-parity orbits leads to the fragmentation of the angular-momentum alignments over many quasiparticle states. Consequently, many quasiparticles have similar alignments so that the probability of occurrence of IBs increases.

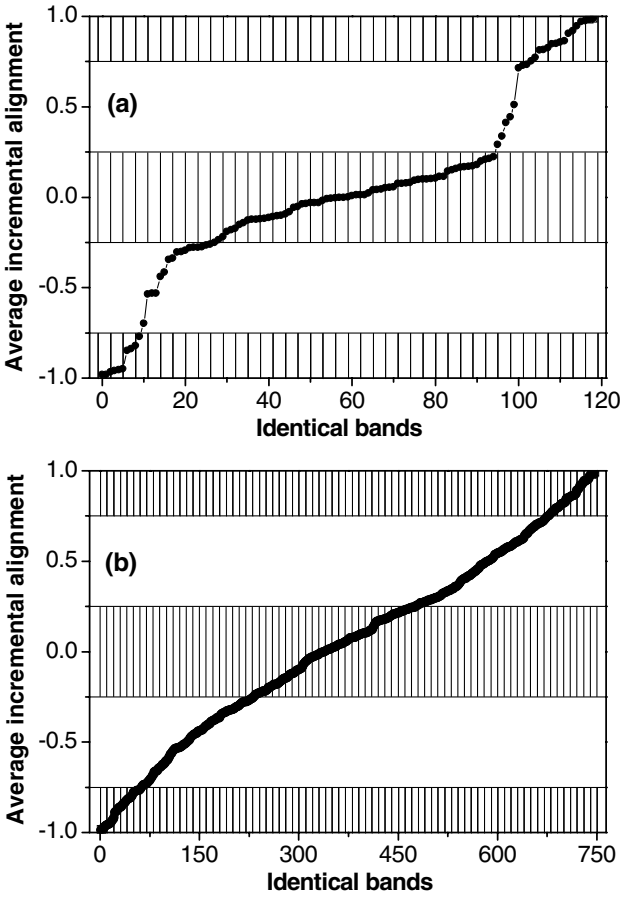

Fig. 2. The distributions of the average incremental alignments for SD IBs in the $A = 190$ mass region: (a) for 119 IBs found when $N = 11$, $\delta = 0.6$ keV, (b) for 746 IBs found when $N = 11$, $\delta = 1.4$ keV. The quantization regions are shaded.

4.2 The quantization behavior of the incremental alignment of IBs

In the following discussion, we shall concentrate on the quantization property of the incremental alignment of IBs. We shall see that the quantization behavior of incremental alignment is very different in SD and ND nuclei, in a manner of statistics. In the present analysis, the parameter N will be restricted to 7 (11) in ND (SD) nuclei and δ

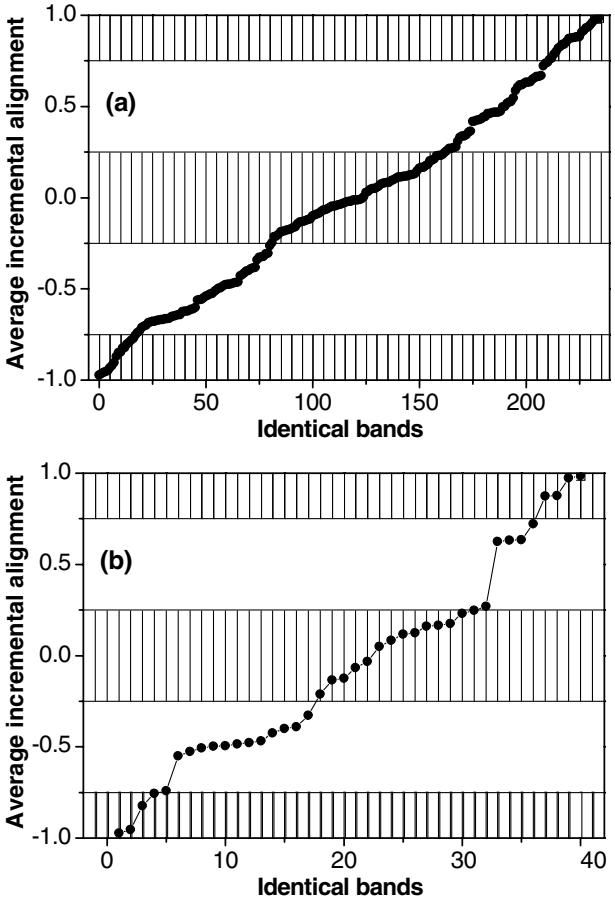

Fig. 3. The distributions of the average incremental alignments for ND IBs in the rare-earth region ($A = 160$ mass region): (a) for 235 IBs found when $N = 7$ and $\delta = 1.6$ keV, (b) for 40 IBs found when $N = 7$ and $\delta = 0.8$ keV. The quantization regions are shaded.

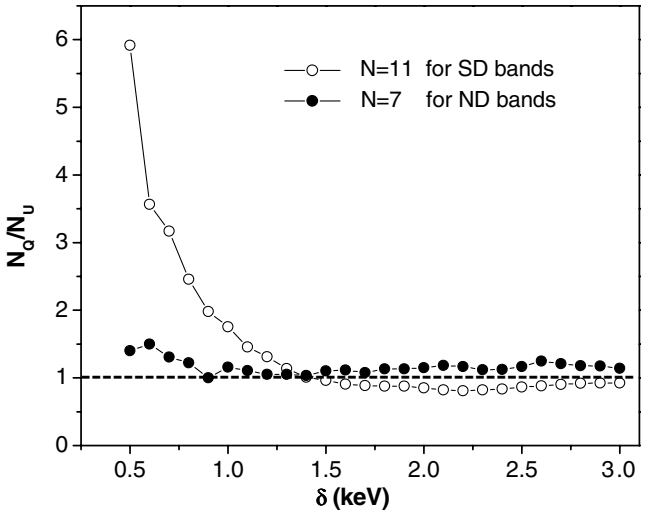

Fig. 4. The ratio N_Q/N_U varies against δ. The solid (open) circles are for normal- (super-) deformed nuclei and $N = 7$ (11).

remains a varying parameter. The distributions of $\overline{\Delta i}$ for SD IBs in the $A = 190$ region and ND IBs are shown in fig. 2 and fig. 3 respectively.

For the SD bands in the $A = 190$ region, there are 119 pairs of IBs found with the criterion $\delta = 0.6$ keV and 746 pairs of IBs found with $\delta = 1.4$ keV. In fig. 2a, there are 93 incremental alignments located in the Q region (shaded) and 26 in U region (unshaded), the ratio $N_Q/N_U = 3.58$. While in fig. 2b, there are 375 incremental alignments located in the Q region and 371 in the U region, $N_Q/N_U = 1.01$. Thus, the ratio N_Q/N_U is strongly related to the strictness of the criterion for IBs. For a given N, a small δ favors the quantization of the incremental alignment. The quantized incremental alignment between pairs of IBs in nuclei of the same type (both even mass or both odd mass) is integer (including zero), and is half-integer between bands in nuclei of different types [16]. In fig. 2a, most of the incremental alignments are located around zero.

Figure 3 shows the distributions of the average incremental alignments for the calculated ND IBs in the rare-earth region. There are 235 pairs of IBs found with the criterion of $N = 7$ and $\delta = 1.6$ keV. In fig. 3a, 124 incremental alignments are located in the Q region and 111 in the U region, the ratio $N_Q/N_U = 1.112$. For a more strict criterion $\delta = 0.8$ keV, there are 40 pairs of IBs found and their incremental alignments are plotted in fig. 3b. From fig. 3b one can see that there are 21 incremental alignments located in the Q region and 19 in the U region, and the ratio N_Q/N_U equals 1.105. The ratio $N_Q/N_U \approx 1$ means that the number of IBs with quantized alignments is almost equal to the number of IBs having unquantized alignments, and this implies that the incremental alignments are kept unquantized in ND nuclei even with a strict statistical criterion.

In fig. 4 the ratio N_Q/N_U is plotted as a function of δ for the ND IBs (solid circles) and SD IBs (open circles). The selecting criterion N is equal to 7 for ND bands and to 11 for SD bands. It is seen that the ratio for normal-deformed IBs is almost a constant near 1, and thus presents the feature of unquantized alignments of IBs. In contrast, for superdeformed IBs the ratio is almost the same as that for normal-deformed IBs when δ >1.4 keV, but the ratio increases drastically with decreasing δ, namely, when the criterion δ becomes strict, the incremental alignment in SD IBs presents the feature of quantization. The result shown in fig. 4 is very close to that shown in fig. 2 of ref. [12] where the experimental rotational bands were analyzed in the same way. This similarity implies that the quantization behavior of the incremental alignments observed from the experiments is reproduced by the present theoretical simulation. From the point of view of statistics, we may conclude that the incremental alignments are quantized for SD IBs but unquantized for ND IBs. We should mention that the result is preliminary and the mechanism of the quantization in SD nuclei is still an open question. We expect to get the answer to this problem by analyzing the single-particle structure with the RASM in another paper.

5 Summary

In summary, the properties of IBs are investigated by analyzing a large number of rotational bands produced with the reflection asymmetric shell model. The theoretical simulations show that there exists a large excess of IBs in SD nuclei compared to the ND nuclei, and the distribution functions of the calculated $J^{(2)}$ and E_γ also support this conclusion. Furthermore, the octupole effect on the identical bands is discussed, and the result shows that the frequency of occurrence of superdeformed IBs increases when the octupole deformation is switched on. From the present theoretical simulations, we may conclude that more correlations lead to more IBs.

The frequency of occurrence and the behaviors of IBs, such as the quantization of incremental alignments, revealed in the experiment, have been generally reproduced by the present theoretical simulation. This would indicate that the nuclear mean-field approximation plus the beyond mean-field one, like angular-momentum and parity projections, can reproduce the phenomena of IBs even though there is no available theory that can reach the accuracy of identity between the specific identical bands.

The work was supported by the National Natural Science Foundation of China under Grants Nos. 10235020, 10305019 and 10475115.

References

1. T. Byrski *et al.*, Phys. Rev. Lett. **64**, 1650 (1990).
2. F.S. Stephens *et al.*, Phys. Rev. Lett. **64**, 2623 (1990).
3. F.S. Stephens *et al.*, Phys. Rev. Lett. **65**, 301 (1990).
4. I. Ahmad *et al.*, Phys. Rev. C **44**, 1204 (1991).
5. C. Baktash, B. Hass, W. Nazarewicz, Annu. Rev. Nucl. Part. Sci. **45**, 485 (1995) and references therein.
6. G. de France *et al.*, Phys. Rev. C **53**, R1070 (1996).
7. B.K. Lennart *et al.*, Phys. Lett. B **416**, 16 (1998).
8. Y.S. Chen, Z.C. Gao, Phys. Rev. C **63**, 014314 (2000).
9. G. Hackman *et al.*, Phys. Rev. Lett. **79**, 4100 (1997).
10. T. Lauritsen *et al.*, Phys. Rev. Lett. **89**, 282501 (2002).
11. C.W. Shen, W.D. Luo, Y.S. Chen, Phys. Rev. C **55**, 1762 (1997).
12. C.W. Shen, Y.S. Chen, Phys. Rev. C **58**, 2081 (1998).
13. K. Hara, Y. Sun, Int. J. Mod. Phys. E **4**, 637 (1995).
14. T. Bengtsson, I. Ragnarsson, Nucl. Phys. A **436**, 14 (1985).
15. F.S. Stephens, Nucl. Phys. A **520**, 91c (1990).
16. F.S. Stephens *et al.*, Phys. Rev. C **57**, R1565 (1998).
17. P.A. Bulter, W. Nazarewicz, Rev. Mod. Phys. **68**, 349 (1996).